Journal of Geosciences, 54 (2009), 355–371 DOI: 10.3190/jgeosci.055

Original paper

Cu-rich members of the beudantite–segnitite series from the Krupka ore district, the Krušné hory Mountains, Czech Republic

Jiří SEJKORA[1]*, Jiří ŠKOVÍRA[2], Jiří ČEJKA[1], Jakub PLÁŠIL[1]

[1] *Department of Mineralogy and Petrology, National museum, Václavské nám. 68, 115 79 Prague 1, Czech Republic; jiri_sejkora@nm.cz*
[2] *Martinka, 417 41 Krupka III, Czech Republic*
[*] *Corresponding author*

Copper-rich members of the beudantite–segnitite series (belonging to the alunite supergroup) were found at the Krupka deposit, Krušné hory Mountains, Czech Republic. They form yellow-green irregular to botryoidal aggregates up to 5 mm in size. Well-formed trigonal crystals up to 15 μm in length are rare. Chemical analyses revealed elevated Cu contents up to 0.90 *apfu.* Comparably high Cu contents were known until now only in the plumbojarosite–beaverite series. The Cu^{2+} ion enters the B^{3+} position in the structure of the alunite supergroup minerals via the heterovalent substitution $Fe^{3+}Cu^{2+}_{-1} \rightarrow (AsO_4)^{3-}(SO_4)^{2-}_{-1}$. The unit-cell parameters (space group *R*-3*m*) *a* = 7.3265(7), *c* = 17.097(2) Å, *V* = 794.8(1) Å^3 were determined for compositionally relatively homogeneous beudantite (0.35 – 0.60 *apfu* Cu) with the following average empirical formula: $Pb_{1.00}(Fe_{2.46}Cu_{0.42}Al_{0.13}Zn_{0.01})_{\Sigma 3.02}[(SO_4)_{0.89}(AsO_3OH)_{0.72}(AsO_4)_{0.34}(PO_4)_{0.05}]_{\Sigma 2.00}[(OH)_{6.19}F_{0.04}]_{\Sigma 6.23}$. Interpretation of thermogravimetric and infrared vibrational data is also presented. The Cu-rich members of the beudantite–segnitite series are accompanied by mimetite, scorodite, pharmacosiderite, cesàrolite and carminite. These minerals are characterized by refined unit-cell parameters and by quantitative chemical analyses. The assemblage of supergene minerals corresponds to the following crystallization sequence: mimetite → beudantite–segnitite → pharmacosiderite, scorodite, cesàrolite, and carminite.

Keywords: beudantite, segnitite, Cu content in members of alunite supergroup, thermogravimetric data, infrared spectroscopy, Krupka deposit
Received: 7 October 2009; accepted 18 December 2009; handling editor: M. Novák

The online version of this article (doi: 10.3190/jgeosci.055) contains supplementary electronic material.

1. Introduction

Various aspects of mineralogy and chemistry of Pb and As–S dominated members of the alunite supergroup have attracted attention in the last two decades. Examples include importance in ore dressing (Dutrizac and Jambor 2000; Jiang and Lawson 2006), in environmental studies (e.g. Dutrizac and Dinardo 1983; Alpers et al. 1989; Dutrizac et al. 1996; Sasaki and Konno 2000; Morin et al. 2001; Kolitsch and Pring 2001), and the recognition of jarosite presence on the surface of Mars (Klingelhöfer 2004). This situation warranted a detailed and complex study of locally abundant assemblage including Cu-rich members of the beudantite–segnitite series (alunite supergroup) in the Krupka ore district.

This paper is a part of the systematic research of a large group of supergene minerals (Sejkora et al. 2007a, 2009; Plášil et al. 2009a–c).

2. Characteristics of the occurrence

The historical Krupka ore district is located northwest of the town of Teplice in the Krušné hory Mts. (northern Bohemia, Czech Republic). The district extends from the most elevated part in the Komáří Vížka area to the outskirts of Bohosudov and into the vicinity of the Unčín village. Mineralogical information and geological and montanistic characteristics of the district were presented by Sejkora and Breiter (1999). Several recent studies gave information on abundant occurrences of supergene mineralization of Cu, Zn and Pb (Škovíra et al. 2004; Sejkora et al. 2007b; Sejkora and Škovíra 2007; Sejkora et al. 2008), which were previously unknown.

The first isolated finds of Cu-rich members of the beudantite–segnitite series originate from dumps dispersed in the forest above the Stříbrná (Gotteskinder) adit, *c.* 50 to 70 m from the northern margin of Krupka. Later on,

occurrences of these minerals were found in an old adit about 10 m below land surface, in a steep tectonised zone up to 30 cm wide, showing a strong supergene alteration. In addition to supergene minerals of Pb, Cu and Fe, this zone and the adjacent rocks contain quartz and clay minerals with relics of primary ore minerals including galena, arsenopyrite, cassiterite and wolframite.

3. Analytical techniques

The surface morphology of samples was studied with a Nikon SMZ1500 optical microscope in combination with a Nikon DXM1200F digital camera, used for photography in incandescent light. Details of surface morphology of gold-coated samples were studied with a JEOL JSM-6380 electron scanning microscope (SEM).

If not stated otherwise, all minerals described in this paper were identified by X-ray powder diffraction analysis. The samples studied were placed on the surface of a flat silicon wafer from suspension in ethanol. Step-scanned powder diffraction data were collected using a HZG4-AREM/Seifert diffractometer with a copper tube, operated at 50 kV and 40 mA. The results were processed using the X-ray analysis software ZDS for DOS (Ondruš 1993), Bede ZDS Search/Match ver. 4.5 (Ondruš and Skála 1997), and unit-cell parameters were refined with the program of Burnham (1962).

Quantitative chemical data were collected with a Cameca SX100 electron microprobe (Laboratory of Electron Microscopy and Microanalysis of the Masaryk University and Czech Geological Survey, Brno) operating in the wavelength-dispersion mode with an accelerating voltage of 15 kV, a specimen current of 8–10 nA, and a beam diameter of 5–10 μm. The following lines and standards were used: K_α: andradite (Ca, Fe), albite (Na), barite (S), sanidine (Al, Si, K), fluorapatite (P), ZnO (Zn), olivine (Mg), rhodonite (Mn), vanadinite (V), topaz (F), halite (Cl); L_α: InAs (As), dioptase (Cu), Sb (Sb); M_α: vanadinite (Pb) and M_β: Bi (Bi). Peak counting times (CT) were 20 s for main elements and 60 s for minor elements; CT for each background was ½ of peak time. Raw intensities were converted to the concentrations using automatic *PAP* (Pouchou and Pichoir 1985) matrix correction software package. Elevated analytical totals of minerals containing a large amount of hydroxyl groups or crystal water are generally caused by water evaporation under high-vacuum conditions or water evaporation due to heating of the analyzed spot by the electron beam. Lower analytical totals for some samples are primarily caused by their porous nature or by poorly polished surfaces of soft or cryptocrystalline minerals.

Thermogravimetric analysis was carried out with a Stanton Redcroft TG 750 Thermobalance. The sample of compositionally relatively homogeneous Cu-rich beudantite (weight 0.986 mg) was heated from room temperature to 950 ºC at a heating rate 10 °C min^{-1} in flowing air (10 ml min^{-1}). Infrared spectra were recorded by the micro-DRIFTS method on a Nicolet Magna 760 FTIR spectrometer (range 4000–600 cm^{-1}, resolution

Fig. 1 Yellow-green crystalline crusts of Cu-rich beudantite, Krupka. Width of the area 2 mm. Photograph by J. Sejkora.

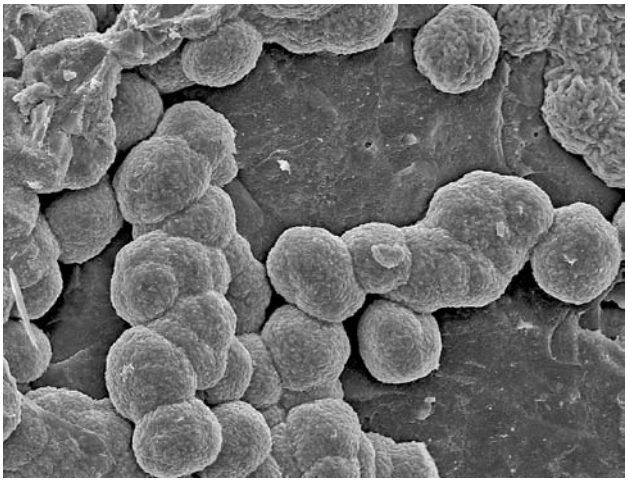

Fig. 2 Hemispherical microcrystalline aggregates of Cu-rich beudantite. Width of the area 100 μm. Back-scattered electron (BSE) photograph by J. Sejkora.

4 cm^{-1}, 128 scans, 2 level zero-filtering, Happ–Genzel apodization), equipped with a Spectra Tech InspectIR micro FTIR accessory. The samples, each weighing less than 0.050 mg, were mixed without using pressure with KBr. Samples were immediately recorded with the same KBr as a reference.

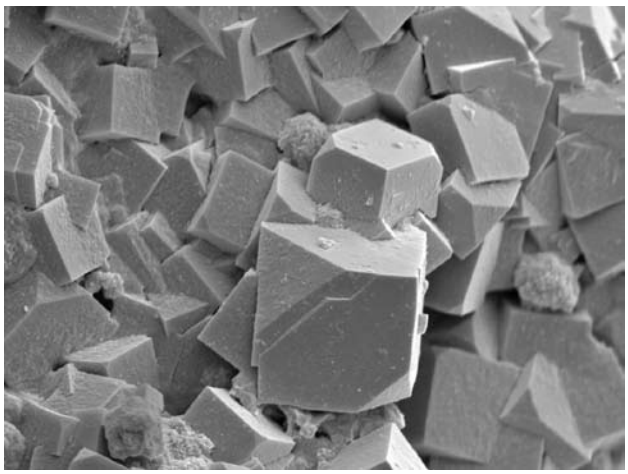

Fig. 3 Group of pseudo-cubic to pseudo-cuboctahedral crystals of Cu-rich beudantite, Krupka. Width of the area 60 µm. The BSE photograph by J. Sejkora.

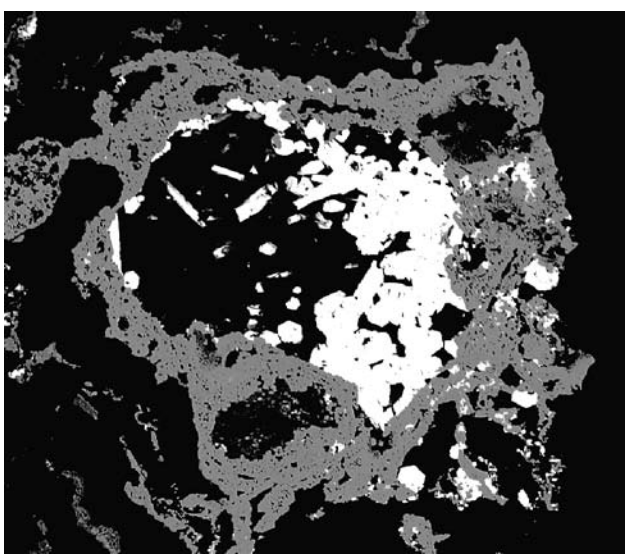

Fig. 4 Crystalline aggregate of mimetite (white) overgrown by a crystalline aggregate of Cu-rich beudantite, Krupka. Width of the area 600 µm. The BSE photograph by J. Sejkora.

4. Beudantite–segnitite solid solution series

4.1. Description of samples

Cu-rich members of the beudantite–segnitite series form yellow green irregular aggregates (Fig. 1), 3–5 mm in diameter, partly filling voids in weathered and leached primary ore minerals. These minerals also occur as thin coatings (0.1–0.2 mm) on fracture surfaces in gangue and in silicified wall rock. The surface of beudantite–segnitite series aggregates is irregular and nearly smooth; in places are recognizable minor botryoidal aggregates including local hemispherical shapes up to 20 µm in diameter (Fig. 2). Well-formed pseudocubic crystals, 5–15 µm across (Fig. 3), are confined to rare minute cavities. Both macroscopic and microscopic observations indicate that the beudantite–segnitite series minerals overgrew and replaced older crystals and aggregates of mimetite (Fig. 4). They are accompanied by younger pharmacosiderite, scorodite, cesàrolite and carminite.

4.2. Chemical composition

Members of the beudantite–segnitite solid solution series represent a small part of the large supergroup of natural

dominant elements	Na^{+}			
	K^{+}			
	H_3O^{+}			
	Ag^{+}			
	NH_4^{+}			
	Tl^{+}			
	Pb^{2+}			
	Ca^{2+}		$(SO_4)^{2-}$	
	Ba^{2+}	Al^{3+}	$(AsO_3OH)^{2-}$	
	Sr^{2+}	Fe^{3+}	$(PO_3OH)^{2-}$	
	Bi^{3+}	V^{3+}	$(AsO_4)^{3-}$	
	$LREE^{3+}$	Ga^{3+}	$(PO_4)^{3-}$	$(OH)^{-}$
	***A*-site**	***B*-site**	***T*-site**	***X*-site**
minor elements or synthetic phases	Cs^{+}	Cu^{2+}	$(SeO_4)^{2-}$	Cl^{-}
	Rb^{+}	Zn^{2+}	$(CO_3)^{2-}$	F^{-}
	Mg^{2+}	Co^{2+}	$(CrO_4)^{2-}$	H_2O
	Hg^{2+}	Ni^{2+}	$(WO_4)^{2-}$	
	UO_2^{2+}	Mg^{2+}	$(SiO_4)^{4-}$	
	Th^{4+}	Mn^{2+}		
	U^{4+}	Cr^{3+}		
	Zr^{4+}	In^{3+}		
		Sc^{3+}		
		Ti^{4+}		
		Ge^{4+}		
		Sb^{5+}		
		Ta^{5+}		
		Nb^{5+}		
		W^{6+}		

Fig. 5 Elements occurring in the natural and synthetic members of the alunite supergroup, modified following Schwab et al. (2004), with the use of data by Scott (1987), Novák et al. (1994), Kolitsch and Pring (2001) and Pe-Piper and Dolansky (2005).

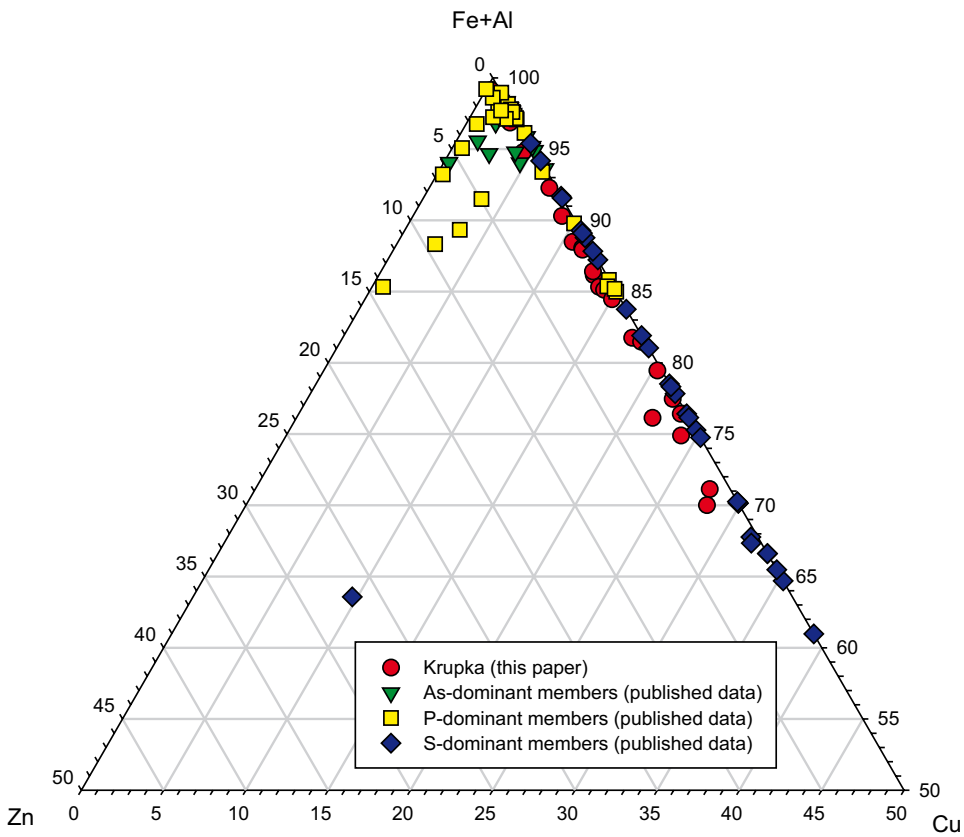

Fig. 6 Part of a ternary plot of Cu – Fe + Al – Zn of *B*-site occupancy (atomic ratio) for Pb-dominant members of alunite supergroup. Data from van Tassel (1958), Taguchi (1961), Morris (1962), Nambu et al. (1964), Taguchi et al. (1972), Slansky (1977), Walenta et al. (1982), Jambor and Dutrizac (1983, 1985), Scott (1987), de Bruiyn et al. (1990), Birch et al. (1992), Breidenstein et al. (1992), Pring et al. (1995), Rattray et al. (1996), Jansa et al. (1998), Sejkora et al. (2001a, 2001b) and Sato et al. (2008).

and synthetic compounds with the alunite-type structure. The chemical composition of the alunite supergroup members can be expressed by the general formula $AB_3(TO_4)_2X_6$ (Scott 1987; Kolitsch and Pring 2001; Sejkora et al. 2006b; Mills 2007; Mills et al. 2009a), whereby *A*-site is occupied by large monovalent (Na, K, Ag, NH_4, H_3O...), divalent (Pb, Ca, Sr, Ba...), trivalent (Bi, LREE...) or tetravalent (Th, Zr...) elements in 12-coordination. At the octahedral *B*-position, trivalent cations (Al, Fe) dominate over divalent (Cu, Zn) or pentavalent (Nb, Ta) cations. At the tetrahedral *T*-sites are present mainly S, P and As, even though minor contents of Si, Cr and other elements were also determined. The hydroxyl groups (OH) dominate in *X*-position over minor amounts of Cl and F; H_2O is also present according to some authors. A general review of possible substitutions in members of the alunite supergroup is presented in Fig. 5.

For $A^{2+}B^{3+}T^{5+}$ members of this group (e.g. plumbogummite Pb–Al–P, segnitite Pb–Fe–As, kintoreite Pb–Fe–P etc.), the charge balance requires protonation of one of TO_4 anions. Consequently, their ideal formula should be written as $AB_3(TO_4)^{3+}(TO_3OH)^{2+}X_6$ (Scott 1987). New structural studies indicate complete disorder of the groups SO_4, PO_4, PO_3OH, AsO_4 and AsO_3OH (Kolitsch and Pring 2001; Dzikowski et al. 2006). Another charge-compensation mechanism (Zn and other elements occupying new sites within six-membered rings in the octahedral layers) was described by Mills et al. (2009b) and Grey et al. (2009).

Minerals of the beudantite–segnitite series from Krupka contain dominating Pb in the range of 0.93–1.13 *apfu* at the *A*-site, accompanied by minor Ca (<0.02 *apfu*). In the *B*-site Fe^{3+} is always the dominant ion (1.92–2.72 *apfu*); minor Al^{3+} (0.03–0.16) and Zn^{2+} (0.01–0.07 *apfu*) are also present. Notable are Cu^{2+} contents in the range of 0.01 to 0.90 *apfu* in the studied samples (Fig. 6). As

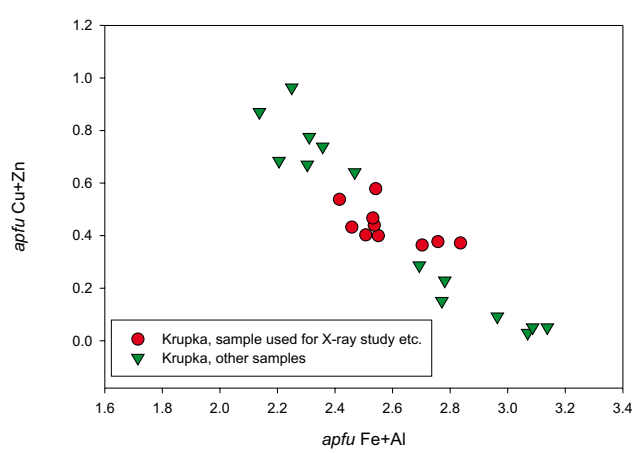

Fig. 7 Plot *apfu* Fe + Al *vs.* *apfu* Cu + Zn for minerals of beudantite–segnitite solid solution series from Krupka.

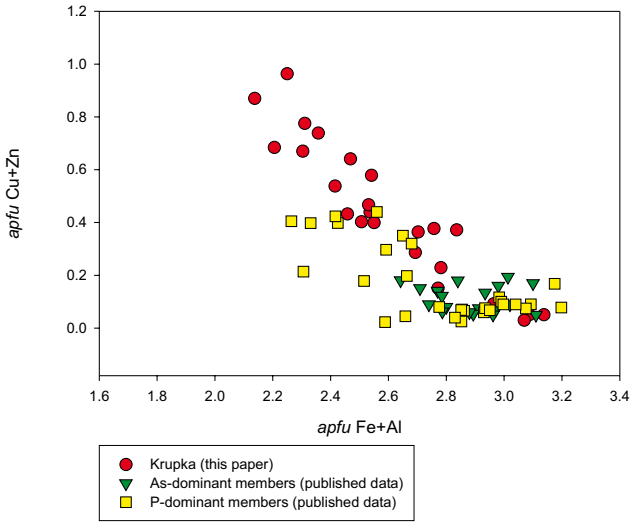

Fig. 8 Plot *apfu* Fe + Al *vs. apfu* Cu + Zn for Pb and As(P) dominant members of alunite supergroup. Data from Nambu et al. (1964), Slansky (1977), Walenta et al. (1982), Scott (1987), de Bruiyn et al. (1990), Birch et al. (1992), Pring et al. (1995), Rattray et al. (1996), Jansa et al. (1998) and Sejkora et al. (2001a, 2001b).

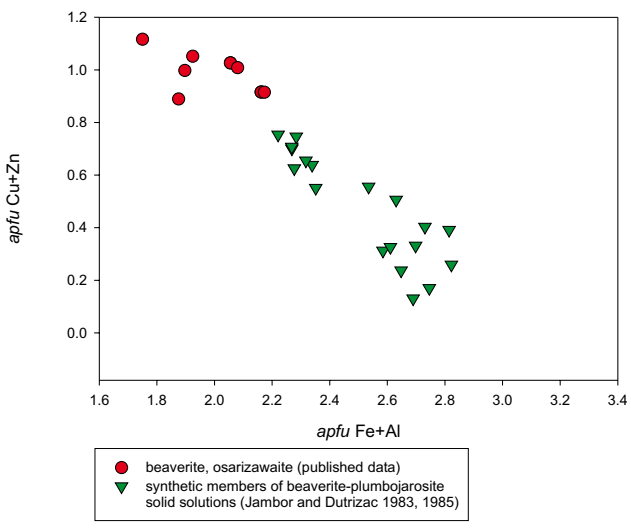

Fig. 9 Plot *apfu* Fe + Al *vs. apfu* Cu + Zn for Pb and S dominant members of alunite supergroup. Data from van Tassel (1958), Taguchi (1961), Morris (1962), Taguchi et al. (1972) and Breidenstein et al. (1992).

indicated by the positive correlation of Cu + Zn with Fe + Al (Fig. 7), Cu^{2+} is positioned in the octahedral *B*-site, similar to the situation with Pb-dominated sulphates of the alunite supergroup – beaverite-(Cu) and beaverite-(Zn) (Taguchi 1961; Morris 1962; Taguchi et al. 1972; Jambor and Dutrizac 1983, 1985; Scott 1987; Sato et al. 2008). In the naturally occurring Pb members of the alunite supergroup, dominated by As or P, comparably high contents of Cu^{2+} in the *B*-site, near to 1/3 of the position, are not indicated (Fig. 8). Comparably high contents were reported only in members dominated by Pb

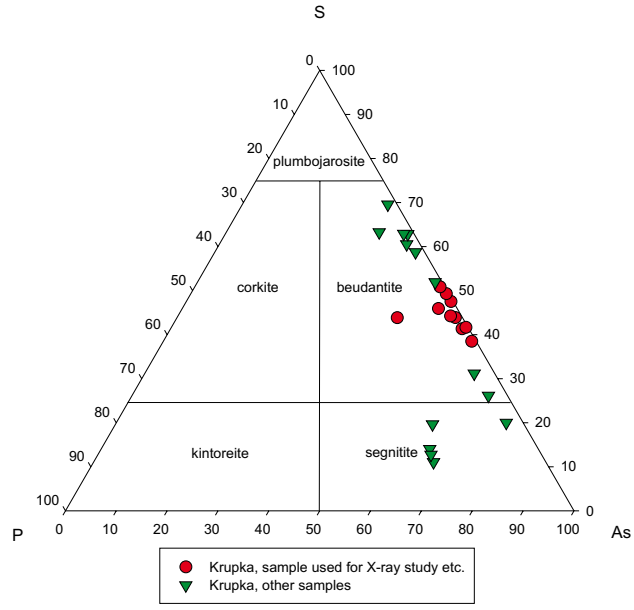

Fig. 10 Ternary plot of As – S – P of *T*-sites occupancy (atomic ratios) for minerals of beudantite–segnitite solid solution series from Krupka.

and S (Fig. 9). It is not possible to exclude that Cu^{2+} can occupy the newly determined trigonal–bipyramidal site, similarly to the case of kolitschite and kintoreite (Mills et al. 2008; Grey et al. 2008, 2009).

The tetrahedral *T*-sites contain 0.72–1.77 As and 0.28–1.38 S *apfu* and minor P (0.01–0.44 *apfu*). As indicated by charge-balance requirements (Pb^{2+} in *A*-sites), a part of As (near 0.72 *apfu*) must be protonated forming the $(AsO_3OH)^{2-}$ group. As follows from Fig. 10, the majority of the studied samples plot in the beudantite field and only several spot analyses represent segnitite. The elevated Cu^{2+} contents in the nominal B^{3+} position are compensated by the heterovalent substitution $Fe^{3+}Cu^{2+}_{-1} \rightarrow (AsO_4)^{3-}(SO_4)^{2-}_{-1}$. A good correlation of Cu^{2+} contents in the *B*-sites and $(SO_4)^{2-}$ in the tetrahedral *T*-sites is shown in Fig. 11.

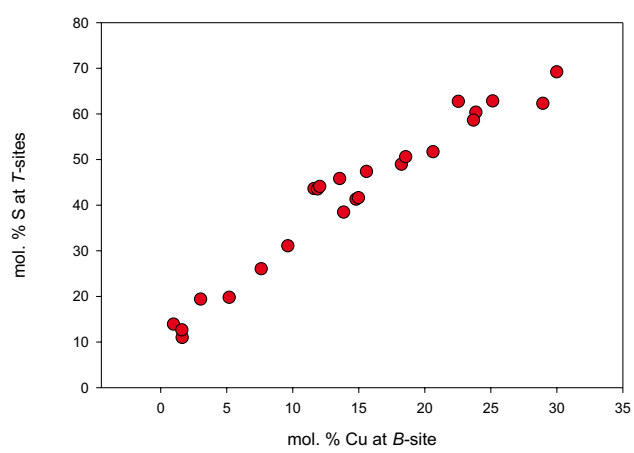

Fig. 11 Plot mol. % Cu at *B*-site *vs.* mol. % S at *T*-sites for minerals of beudantite–segnitite solid solution series from Krupka.

Tab. 1 Chemical composition of minerals of beudantite–segnitite solid solution series from Krupka (wt. %)

	mean	1	2	3	4	5	6	7	8	9	10
CaO	0.03	0.12	0.05	0.04	0.04	0.04	0.04	0.02	0.08	0.07	0.07
BaO	0.03	0.00	0.00	0.00	0.00	0.07	0.07	0.00	0.04	0.00	0.05
PbO	30.18	32.32	31.86	29.30	29.21	28.78	29.96	30.49	30.38	31.44	31.69
CuO	4.50	0.42	0.80	2.30	2.89	4.17	4.45	5.70	7.45	8.98	9.57
MnO	0.03	0.00	0.00	0.02	0.00	0.00	0.00	0.00	0.00	0.00	0.00
ZnO	0.22	0.12	0.17	0.14	0.21	0.24	0.29	0.22	0.12	0.41	0.69
Al_2O_3	0.87	7.75	4.15	2.00	1.96	0.85	0.90	0.66	0.19	1.21	1.09
Fe_2O_3	26.54	20.10	24.85	26.65	26.11	26.85	25.97	25.60	25.79	21.24	22.31
SiO_2	0.05	0.07	0.20	0.04	0.04	0.03	0.00	0.10	0.02	0.15	0.08
As_2O_5	16.40	20.01	18.74	21.56	20.16	15.99	17.81	15.84	11.69	10.83	8.75
P_2O_5	0.47	4.09	3.34	0.71	0.78	0.73	0.26	0.10	0.26	0.39	0.35
SO_3	9.65	2.30	4.12	5.60	6.76	10.16	8.94	10.83	14.25	13.52	14.81
Cl	0.02	0.02	0.03	0.01	0.02	0.02	0.02	0.02	0.02	0.01	0.03
F	0.12	0.66	0.47	0.23	0.24	0.13	0.07	0.07	0.17	0.25	0.26
H_2O*	8.42	8.24	8.18	8.02	8.01	8.27	8.19	8.31	8.71	8.32	8.65
F,Cl=O	–0.05	–0.28	–0.21	–0.10	–0.11	–0.06	–0.03	–0.03	–0.07	–0.11	–0.11
Total	97.47	95.92	96.76	96.52	96.32	96.27	96.92	97.91	99.08	96.70	98.26
Ca^{2+}	0.004	0.016	0.007	0.006	0.005	0.006	0.005	0.002	0.010	0.009	0.009
Ba^{2+}	0.001	0.000	0.000	0.000	0.000	0.003	0.003	0.000	0.002	0.000	0.002
Pb^{2+}	0.999	1.107	1.078	0.979	0.964	0.932	0.993	0.989	0.960	1.039	1.062
Mn^{2+}	0.003	0.000	0.000	0.002	0.000	0.000	0.000	0.000	0.000	0.000	0.000
Σ *A*-site	1.008	1.123	1.085	0.986	0.970	0.940	1.002	0.991	0.971	1.048	1.073
Cu^{2+}	0.418	0.040	0.076	0.216	0.267	0.379	0.414	0.519	0.660	0.833	0.900
Zn^{2+}	0.020	0.011	0.016	0.013	0.019	0.021	0.026	0.019	0.010	0.037	0.064
Al^{3+}	0.126	1.163	0.615	0.293	0.284	0.121	0.130	0.094	0.026	0.174	0.159
Fe^{3+}	2.455	1.924	2.349	2.489	2.409	2.429	2.406	2.322	2.278	1.963	2.091
Σ *B*-site	3.019	3.137	3.056	3.010	2.979	2.950	2.976	2.954	2.974	3.007	3.213
Si^{4+}	0.006	0.009	0.025	0.005	0.005	0.004	0.000	0.012	0.002	0.018	0.009
As^{5+}	1.055	1.331	1.231	1.399	1.293	1.006	1.146	0.998	0.717	0.695	0.570
P^{5+}	0.049	0.440	0.356	0.075	0.080	0.074	0.027	0.010	0.026	0.040	0.036
S^{6+}	0.891	0.220	0.388	0.521	0.622	0.917	0.826	0.980	1.255	1.246	1.384
Σ *T*-sites	2.000	2.000	2.000	2.000	2.000	2.000	2.000	2.000	2.000	2.000	2.000
H^+	6.907	6.993	6.856	6.639	6.552	6.633	6.728	6.681	6.817	6.815	7.185
H*	0.720	0.720	0.720	0.720	0.720	0.720	0.720	0.720	0.720	0.720	0.720
$(OH)^-$	6.190	6.270	6.134	5.917	5.830	5.909	6.008	5.962	6.101	6.097	6.469
Cl^-	0.005	0.005	0.007	0.003	0.005	0.005	0.004	0.004	0.004	0.002	0.005
F^-	0.045	0.264	0.188	0.090	0.092	0.049	0.026	0.026	0.061	0.098	0.102
Σ *X*-site	6.240	6.539	6.328	6.010	5.927	5.963	6.039	5.993	6.166	6.197	6.576

mean – mean of ten spot analyses of chemically relatively homogeneous beudantite, used for a detailed X-ray and spectrometry study; 1–10 – representative spot analyses of Cu-rich beudantite covering a wide range of Cu contents;

H_2O* content calculated on the basis of ideal formula and charge balance;

H* – H^+ bound in the group $(AsO_3OH)^{2-}$ calculated on the basis of charge balance;

Coefficients of empirical formula were calculated on the basis of (As + P + S + Si) = 2 *apfu*.

The *X*-site is dominantly occupied by hydroxyl ions (5.65–6.80 OH *pfu*), minor F (0.02–0.26 *apfu*) and Cl up to 0.01 *apfu*. Total calculated occupancy of this site varies from 5.73 to 6.86 *pfu*.

Representative spot analyses of minerals of the beudantite–segnitite series from Krupka are given in Tab. 1. Also included is an average of ten spot analyses of compositionally relatively homogeneous Cu-rich beudantite used for a detailed powder X-ray, thermogravimetric and spectroscopic study. The empirical formula of this Cu-rich beudantite from Krupka is, on the basis of As + P + S + Si = 2.00, $Pb_{1.00}(Fe_{2.46}Cu_{0.42}Al_{0.13}Zn_{0.01})_{\Sigma 3.02}[(SO_4)_{0.89}(AsO_3OH)_{0.72}(AsO_4)_{0.34}(PO_4)_{0.05}]_{\Sigma 2.00}[(OH)_{6.19}F_{0.04}]_{\Sigma 6.23}$.

4.3. Thermogravimetric data

The crystal chemistry of alunite supergroup compounds was discussed by Kolitsch and Pring (2001) including

thermodynamics and thermal stability. Studies on aspects of the thermochemistry of the Pb-dominant members have been undertaken in the past few years for plumbojarosite (Ózacar et al. 2000; Frost et al. 2005a, 2005c), beaverite (Frost et al. 2008) or arsenian plumbojarosite (Mills et al. 2009c).

Copper-rich beudantite from Krupka (Fig. 12) thermally decomposes in several steps. First, there are two partly overlapping decomposition processes: dehydroxylation approximately up to 510 °C, connected with a ~7.6 wt. % weight loss and AsO_3OH dehydroxylation up to 540 °C (~0.9 wt. %). The total weight loss of 8.50 wt. % in the interval to 540 °C corresponds to the content of 8.42 wt. % H_2O derived from the EPMA data and this is in agreement with Mills et al. (2009c), who reported H_2O loss up to 560 °C for arsenian plumbojarosite. The second step, in the range 540–950 °C, is represented by release of SO_2 (Mills et al. 2009c reported release of SO_2 starting at *c.* 560 °C) and probably also with oxygen release corresponding to decomposition of the arsenate group. According to Mills et al. (2009c), the arsenic is bound in phases of the anglesite-, eulytite- and apatite-type during temperature increase. The Cu-rich beudantite decomposition is not completed up to 950 °C.

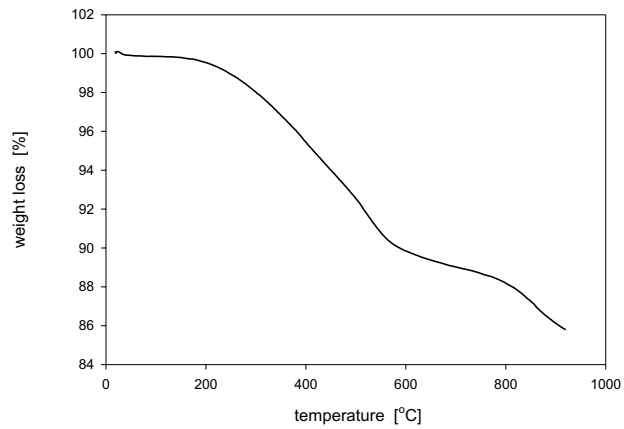

Fig. 12 Thermal analysis of Cu-rich beudantite from Krupka.

Tab. 2 X-ray powder diffraction pattern of Cu-rich beudantite

h	*k*	*l*	$d_{obs.}$	I/I_o	$d_{calc.}$	*h*	*k*	*l*	$d_{obs.}$	I/I_o	$d_{calc.}$
1	0	1	5.943	45	5.948	2	2	0	1.8325	14	1.8316
0	0	3	5.703	6	5.699	2	0	8	1.7717	4	1.7725
1	1	0	3.666	37	3.663	2	2	–3	1.7439	2	1.7438
1	0	4	3.541	8	3.545	2	2	3			1.7438
1	1	3	3.082	100	3.082	2	1	7	1.7115	4	1.7112
1	1	–3			3.082	1	2	–7			1.7112
2	0	2	2.974	16	2.974	1	1	9	1.6866	9	1.6864
0	0	6	2.848	24	2.850	1	1	–9			1.6864
0	2	4	2.548	14	2.547	1	0	10	1.6513	2	1.6509
1	2	–1	2.3722	5	2.3749	0	4	2	1.5594	1	1.5596
2	1	1			2.3749	2	2	–6	1.5412	7	1.5408
2	1	–2	2.3090	6	2.3090	2	2	6			1.5408
1	2	2			2.3090	0	2	10	1.5046	6	1.5051
1	0	7	2.2781	28	2.2794	4	0	4	1.4878	1	1.4871
1	1	6	2.2496	11	2.2492	3	1	–7	1.4277	3	1.4278
1	1	–6			2.2492	1	3	7			1.4278
3	0	0	2.1133	3	2.1150	0	3	9	1.4138	3	1.4133
1	2	–4	2.0886	3	2.0915	3	0	9			1.4133
2	1	4			2.0915	4	1	–3	1.3456	4	1.3454
3	0	3	1.9832	21	1.9828	1	4	3			1.3454
0	3	3			1.9828	1	4	–3			1.3454
2	1	–5	1.9634	1	1.9634	4	1	3			1.3454
1	2	5			1.9634						

4.4. X-ray powder diffraction

The X-ray powder diffraction data for all studied samples of the beudantite–segnitite series from the Krupka ore district (Tab. 2) correspond to the published values for these minerals and to theoretical data calculated from the crystal structure information published for beudantite (Szymański 1988; Giusepetti and Tadini 1989). A sample of relatively chemically homogeneous Cu-rich beudantite was used for refinement of unit-cell parameters; this sample was used for determination of thermogravimetric and vibrational (infrared spectroscopy) data.

The refined unit-cell parameters of the Cu-rich beudantite from the Krupka ore district (Tab. 3) are similar to the published data for As-rich members of the alunite supergroup (beudantite–segnitite – see Fig. 13). The measured and published data for minerals corresponding to the known range of $Cu^{2+} \rightarrow Fe^{3+}$ substitution indicate that the Cu^{2+} contents in *B* position of the ideal formula do not significantly affect unit-cell parameters.

4.5. Infrared spectroscopy

An infrared spectrum was recorded for a sample of compositionally relatively homogeneous Cu-rich beudantite (Fig. 7). It closely compares with the spectrum of beudantite from Cínovec/Zinnwald, Erzgebirge (Sejkora et al. 2001a). The spectrum shows vibration bands corresponding to $(OH)^-$, $(SO_4)^{2-}$, $(AsO_4)^{3-}$ and probably $(AsO_3OH)^{2-}$. In the crystal structure of Cu-rich beudantite, T_d symmetries of free sulphate and arsenate units are lowered and therefore forbidden vibrations may become Raman and/or infrared active and split. The obtained infrared spectrum (Fig. 14, Tab. 4) is tentatively interpreted on the basis of papers by Keller (1971), Vansant et al. (1973), Farmer (1974), Myneni et al. (1998), Sasaki et al.

Tab. 3 Unit-cell parameters of minerals of the beudantite-segnitite solid solution series (for trigonal space group *R*-3*m*)

mineral	occurrence	reference	*a* [Å]	*c* [Å]	*V* [Å³]
Cu-rich beudantite	Krupka	this paper	7.3265(7)	17.097(2)	794.8(1)
beudantite	Tsumeb	Szymański (1988)	7.3151(9)	17.0355(5)	789.5
beudantite	Tsumeb	Szymański (1988)	7.3125(8)	17.0217(7)	788.3
beudantite	Dernbach	Giuseppetti and Tadini (1987)	7.339(1)	17.034(1)	794.6
beudantite	Broken Hill	Rattray et al. (1996)	7.345(7)	17.06(2)	796(2)
beudantite	Broken Hill	Rattray et al. (1996)	7.315(5)	17.07(2)	791(2)
beudantite	Cínovec	Sejkora et al. (2001a)	7.3713(9)	17.076(2)	803.5(1)
beudantite	Moldava	Sejkora et al. (2001a)	7.346(1)	17.012(5)	795.0(3)
beudantite	Moldava	Sejkora et al. (2001a)	7.351(2)	17.028(8)	796.8(5)
segnitite	Schwarzwald	Walenta (1966)	7.36	17.21	807
segnitite	Broken Hill	Birch et al. (1992)	7.359(3)	17.113(8)	802.6(6)
segnitite	Broken Hill	Rattray et al. (1996)	7.335(5)	17.11(2)	797(1)
segnitite	St. Andreasberg	Bischoff (1999)	7.376(1)	17.145(2)	807.8
segnitite	Pützbach, Bad Ems	Bischoff (1999)	7.364(1)	17.145(4)	805.2
segnitite	Cínovec	Jansa et al. (1998)	7.348(3)	17.09(1)	799.1
segnitite	Moldava	Sejkora et al. (2001a)	7.373(1)	17.108(4)	805.4(2)
segnitite	Štěpánov	Sejkora et al. (2001b)	7.382(1)	17.119(3)	807.8(2)
segnitite	Broken Hill	Mills (2007)	7.303	17.108	804.8

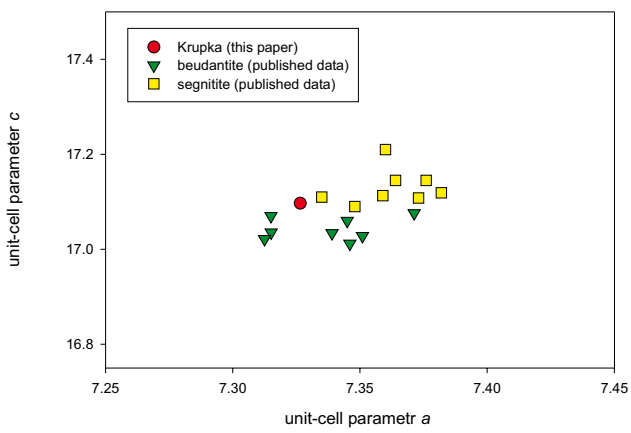

Fig. 13 Plot of unit-cell parameters *a* and *c* for minerals of the beudantite–segnitite series. For published data see Tab. 3.

(1998), Sejkora et al. (2001a), Frost et al. (2005b, 2006) and Murphy et al. (2009).

Broad bands observed at 3362, 3208 and 2924 cm^{-1} are assigned to the ν OH stretching vibrations of hydroxyl ions. Wavenumbers of these ν OH stretching vibrations prove the presence of hydrogen bonds in the crystal structure of Cu-rich beudantite (Libowitzky 1999). There are no vibration bands near 1630 cm^{-1}, which would correspond to deformation vibration of molecular water. The interval 950–1200 cm^{-1} is characterised by a very intense band with maximum at 1037 cm^{-1} featuring numerous shoulders (1172, 1147, 1107, 1079 and 1010 cm^{-1}). A band at 1010 cm^{-1} was assigned to the ν_1 $(SO_4)^{2-}$ symmetric stretching vibration, shoulders at 1172 and 1147 cm^{-1} are attributed to the δ (As–OH) bending vibrations, and bands at 1107, 1079 and 1037 cm^{-1} to the split triply degenerate ν_3 $(SO_4)^{2-}$ antisymmetric stretching vibrations. Some overlapping of these vibrations can be expected. Bands at 935 and 906 cm^{-1} are attributed to the δ M^{3+}–OH bending vibrations. According to the paper by Vansant et al. (1973), bands at 870, 851, 821 and 813 cm^{-1} are assigned to the ν_1 $(AsO_4)^{3-}$ symmetric stretching vibrations and the split triply degenerate ν_3 $(AsO_4)^{3-}$ overlapped with the doubly degenerate ν_3 $(AsO_3OH)^{2-}$ antisymmetric stretching vibrations. A band at 729 cm^{-1} is connected

Tab. 4 Tentative assignment of infrared spectrum of Cu-rich beudantite

assignment	[cm^{-1}]	
ν O-H stretch of hydrogen bonded structurally non-equivalent hydroxyls	3362	m–s
	3208	m
	2924	w
overlapping δ $(AsO_3OH)^{2-}$ bend and ν_3 $(SO_4)^{2-}$ antisymmetric stretch	1172	m
	1147	m
	1107	s
	1079	s
	1037	vs
ν_1 $(SO_4)^{2-}$ symmetric stretch	1010	s
δ M^{3+} – OH bend	935	m
	906	m–s
ν_1 $(AsO_4)^{3-}$ symmetric and ν_3 $(AsO_4)^{3-}$ antisymmetric stretch overlapped with the ν_3 $(AsO_3OH)^{2-}$ antisymmetric stretch	870	s
	851	s
	821	vs
	813	vs
ν_1 $(AsO_3OH)^{2-}$ symmetric stretch	729	w
ν_4 $(SO_4)^{2-}$ bend	687	m
	662	w
	620	m

Intensity of bands: vs – very strong, s – strong, m – medium, w – weak.

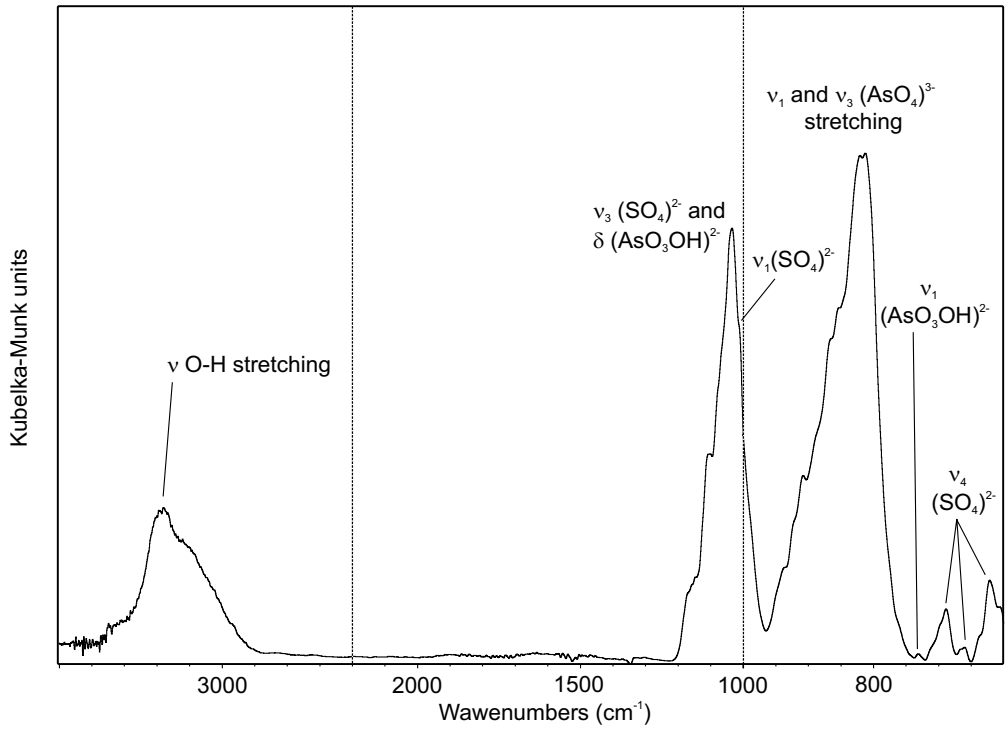

Fig. 14 Micro-DRIFTS spectrum of Cu-rich beudantite from Krupka with assigned bands.

with the ν (As–OH) symmetric stretching vibration and those at 687, 662 and 620 cm^{-1} to the split triply degenerate ν_4 $(SO_4)^{2-}$ bending vibration.

5. Other minerals identified in the association

5.1. Mimetite

In the studied samples, mimetite typically forms porous or compact pseudomorphs after galena up to 0.5 cm across. Some samples contain evidence of early mimetite crystallization along cleavage planes of galena (Fig. 15), followed by complete leaching of galena at a later stage. On rare instances mimetite occurs as well-formed white acicular crystals up to 0.4 mm long, grouped in random clusters (Fig. 16) or making up radiating aggregates 1 to 1.5 mm in diameter (Fig. 17). Mimetite is the oldest supergene mineral in the studied association.

Mimetite was identified by X-ray powder diffraction. Its refined unit-cell parameters, a = 10.2395(6), c = 7.4380(8) Å and V = 675.37(8) $Å^3$, are in agreement with the data published by Baker (1966), Dai and Hughes (1989), Dai et al. (1991), Hashimoto and Matsumoto (1998) as well as Števko et al. (2008) for minerals of the mimetite–pyromorphite solid solution series.

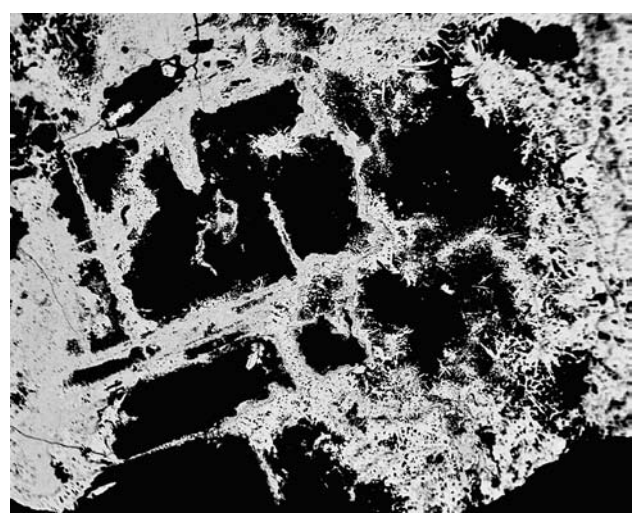

Fig. 15 Mimetite aggregates growing along former cleavage planes of galena, which was completely leached. Krupka. Width of the area 2 mm. The BSE photograph by J. Sejkora.

The chemical analyses of mimetite from Krupka (Tab. 5) correspond to the presence of 0.04–0.29 *apfu* P in the tetrahedral site (PAs_{-1} substitution in the mimetite–pyromorphite series), in addition to dominating As, and sulphur contents up to 0.14 *apfu* S, (heterovalent substitution $As^{5+}S^{6+}_{-1}$). The predominant chlorine in the *X*-site (0.70–0.93 *apfu* Cl) is accompanied by somewhat increased F up to 0.11 *apfu*. The empirical formula of the

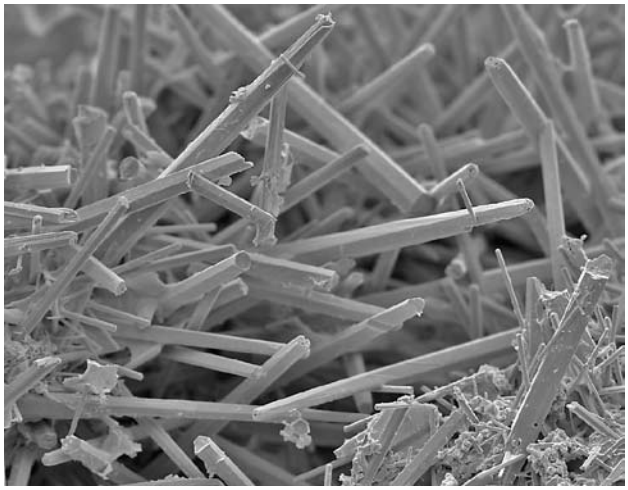

Fig. 16 Aggregate of randomly oriented acicular mimetite crystals. Krupka. Width of the area 150 μm. The BSE photograph taken by J. Sejkora.

Fig. 17 Radiating aggregates of white acicular crystals of mimetite on quartz gangue. Krupka. Width of the area 2.5 mm. Photograph by J. Sejkora.

Tab. 5 Chemical composition of mimetite (wt. %)

	mean	1	2	3	4	5	6
CaO	0.02	0.04	0.01	0.02	0.00	0.01	0.04
FeO	0.22	0.02	0.94	0.10	0.10	0.02	0.16
PbO	75.27	74.64	74.90	75.01	75.45	75.83	75.79
ZnO	0.04	0.01	0.04	0.03	0.08	0.00	0.09
Al_2O_3	0.05	0.02	0.20	0.08	0.01	0.00	0.02
SiO_2	0.04	0.04	0.14	0.05	0.00	0.00	0.02
As_2O_5	22.44	22.35	21.58	22.22	23.70	23.41	21.36
P_2O_5	0.54	0.24	0.81	0.33	0.18	0.28	1.43
SO_3	0.47	0.51	0.76	0.54	0.12	0.46	0.41
Cl	2.08	1.72	2.22	1.69	2.28	2.35	2.23
F	0.13	0.14	0.15	0.14	0.15	0.10	0.13
Cl=O	–0.47	–0.39	–0.50	–0.38	–0.51	–0.53	–0.50
F=O	–0.06	–0.06	–0.06	–0.06	–0.06	–0.04	–0.05
Total	100.79	99.29	101.18	99.77	101.48	101.90	101.12
Ca^{2+}	0.005	0.009	0.003	0.004	0.000	0.003	0.010
Fe^{2+}	0.045	0.005	0.186	0.021	0.019	0.004	0.032
Pb^{2+}	4.831	4.897	4.771	4.906	4.823	4.777	4.817
Zn^{2+}	0.007	0.002	0.007	0.006	0.014	0.000	0.016
Al^{3+}	0.015	0.005	0.055	0.023	0.002	0.000	0.005
Σ Pb-site	4.903	4.918	5.022	4.960	4.859	4.784	4.880
Si^{4+}	0.010	0.010	0.033	0.013	0.000	0.000	0.005
As^{5+}	2.797	2.848	2.670	2.822	2.942	2.864	2.636
P^{5+}	0.110	0.050	0.162	0.067	0.037	0.055	0.286
S^{6+}	0.083	0.093	0.135	0.098	0.021	0.080	0.073
Σ T-site	3.000	3.000	3.000	3.000	3.000	3.000	3.000
Cl	0.842	0.712	0.891	0.696	0.918	0.934	0.892
F	0.101	0.108	0.115	0.106	0.109	0.076	0.096
Σ Cl+F	0.943	0.820	1.006	0.802	1.027	1.010	0.988

mean and 1–6 spot analyses of mimetite from Krupka.
Coefficients of empirical formula were calculated on the basis of (P + As + Si + S) = 3.

analysed mimetite (average of six spot analyses) based on (As + P + Si + S) = 3 is: $(Pb_{4.83}Fe_{0.04}Al_{0.02}Zn_{0.01})_{\Sigma 4.90}[(AsO_4)_{2.80}(PO_4)_{0.11}(SO_4)_{0.08}(SiO_4)_{0.01}]_{\Sigma 3.00}(Cl_{0.84}F_{0.10})_{\Sigma 0.94}$.

5.2. Scorodite

Scorodite is a rather rare mineral in the studied association. It was found only in some samples in the form of whitish to grey–white, rather loose earthy aggregates up to 0.1 mm in size, in association with pharmacosiderite and minerals of the beudantite–segnitite series. Due to rarity and small size of the scorodite aggregates, they could not be studied by X-ray diffraction. Chemical composition of this mineral from Krupka (Tab. 6) corresponds to scorodite; major elements are accompanied by very minor admixture of other elements. The empirical formula for scorodite calculated as average from three spot analyses on the basis (As + P + V + S) = 1 is: $(Fe_{0.89}Al_{0.06}Cu_{0.02}Zn_{0.01})_{\Sigma 0.98}[(AsO_4)_{0.99}(PO_4)_{0.01}]_{\Sigma 1.00}\ .2H_2O$.

5.3. Pharmacosiderite

Pharmacosiderite occurs in a form of pale green coatings, 3 by 5 cm in size, along fractures of altered quartz gangue. The surface of the coatings is irregular passing to botryoidal shapes 1–2 mm in diameter, with rare hexahedral crystals 3–8 μm long, observed in small crevices (Fig. 18). Pharmacosiderite aggregates often enclose small flakes of illite and scorodite and minerals of the beudantite–segnitite series.

Pharmacosiderite was identified by X-ray powder diffraction. Its refined unit-cell parameter, a = 7.9801

Tab. 6 Chemical composition of scorodite (wt. %)

	mean	1	2	3
CaO	0.03	0.06	0.02	0.01
BaO	0.04	0.00	0.03	0.10
PbO	0.29	0.26	0.29	0.32
CuO	0.58	1.05	0.49	0.20
ZnO	0.23	0.21	0.20	0.27
Al_2O_3	1.26	1.06	1.20	1.52
Fe_2O_3	29.97	30.13	30.54	29.25
As_2O_5	48.07	47.67	48.67	47.86
P_2O_5	0.23	0.19	0.32	0.20
V_2O_5	0.03	0.03	0.02	0.04
SO_3	0.04	0.06	0.00	0.06
H_2O*	15.22	15.08	15.43	15.15
Total	95.99	95.80	97.20	94.97
Ca^{2+}	0.001	0.003	0.001	0.000
Ba^{2+}	0.001	0.000	0.000	0.002
Pb^{2+}	0.003	0.003	0.003	0.003
Cu^{2+}	0.017	0.031	0.014	0.006
Zn^{2+}	0.007	0.006	0.006	0.008
Al^{3+}	0.059	0.050	0.055	0.071
Fe^{3+}	0.889	0.901	0.893	0.871
Σ Fe-site	0.976	0.994	0.973	0.962
As^{5+}	0.990	0.991	0.989	0.991
P^{5+}	0.008	0.006	0.010	0.007
V^{5+}	0.001	0.001	0.000	0.001
S^{6+}	0.001	0.002	0.000	0.002
Σ T-site	1.000	1.000	1.000	1.000
H_2O	2.000	2.000	2.000	2.000

Mean and 1–3 – spot analyses of scorodite from Krupka.
Coefficients of empirical formula were calculated on the basis of (P + As + S + V) = 1;
*H_2O content was calculated from the ideal content in the formula H_2O = 2.

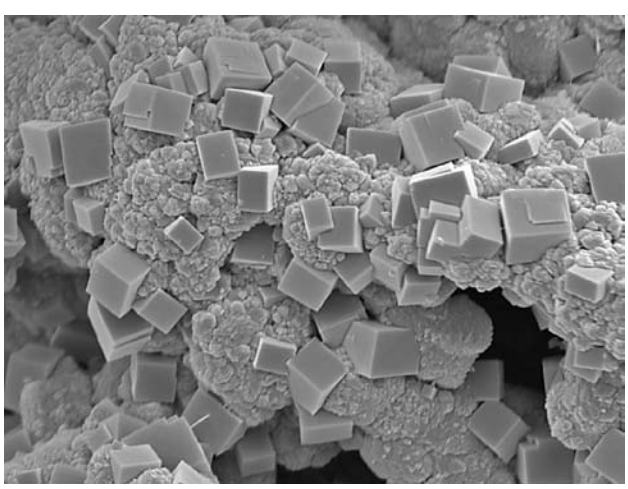

Fig. 18 Cube-shaped pharmacosiderite crystals deposited on finely crystalline aggregate of Cu-rich beudantite. Width of the area 35 µm. The BSE photograph by J. Sejkora.

Å (V = 508.2(1) Å^3), is in agreement with the data published by Buerger et al. (1967). The chemical formula for pharmacosiderite has previously been given as $KFe_4(AsO_4)_3(OH)_4$ .6–7H_2O. Studies by Mutter et al. (1984) with Peacor and Dunn (1985) indicated K (+ Na and Ba) contents in K-site near to 2 *apfu*. Pharmacosiderite from Krupka exhibits total occupancy of the K-site in the range 1.95–2.41 *apfu* (Fig. 19). The variation in K-site occupancy depends on the pharmacosiderite crystal structure, which consists of an open zeolitic framework $[Fe_4(OH)_4(AsO_4)_3]$ – with alkalis, alkaline earths and water molecules in the channels (Buerger et al. 1967). The water content varies considerably and the cations in the channels are considered to be exchangeable (Mutter et al. 1984). Potassium is the dominant element in the K-site of pharmacosiderite samples from Krupka (Fig. 20); the contents of Na and Ba reach maxima of 0.52 and 0.01 *apfu*, respectively. In contrast to the majority of published pharmacosiderite analyses (Fig. 19), the studied samples contain increased Al in the range 0.38–0.53 *apfu* (solid solution with alumopharmacosiderite). Comparably similar elevated Al contents, which enter the structure following a simple substitution $AlFe_{-1}$, were previously reported by Sejkora et al. (2006a). Another characteristic feature of all studied samples from Krupka is a significant content of Si (0.16–0.26 *apfu*), as yet known only in synthetic members (Ti–Si, Ge–Si) of this group (Behrens et al. 1998; Yakovenchuk et al. 2008). Empirical formulae for representative spot analyses of pharmacosiderite from Krupka are given in Tab. 7.

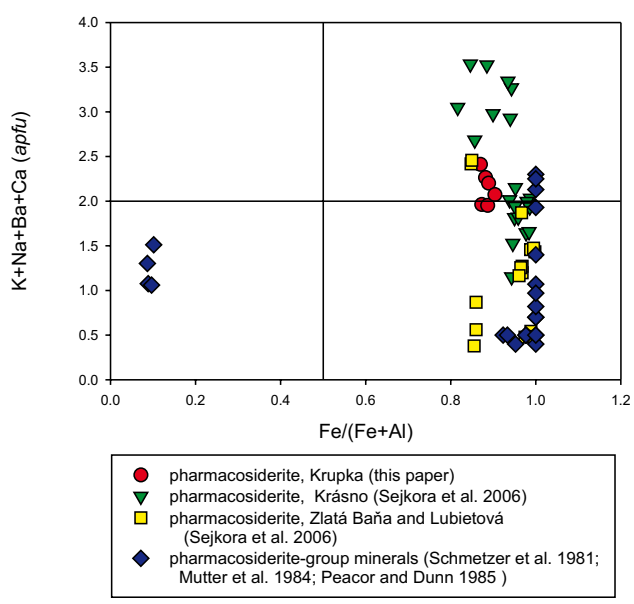

Fig. 19 Plot of Fe/(Fe + Al) vs. (K + Na + Ba + Ca) in K-site of pharmacosiderite from Krupka.

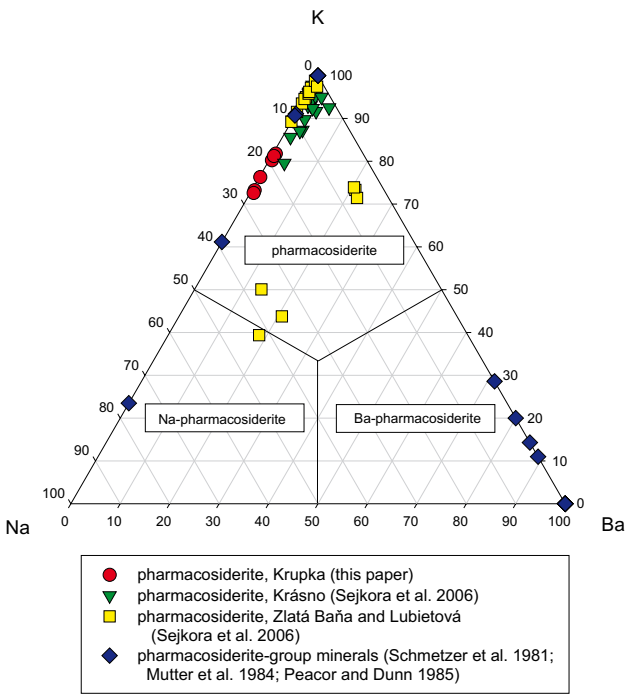

Fig. 20 Ternary plot of K – Na – Ba of K-site occupancy (atomic ratio) for pharmacosiderite from Krupka.

5.4. Carminite

Carminite forms in some samples relatively abundant opaque irregular aggregates of light red-brown to bright red colour (Fig. 21). Carminite aggregates up to 1 mm across are deposited on older minerals of the beudantite–segnitite series. The accumulations are earthy to compact, with a smooth surface, rarely decorated by intergrowth aggregates of elongated tabular crystals up to 2–8 µm long (Fig. 22).

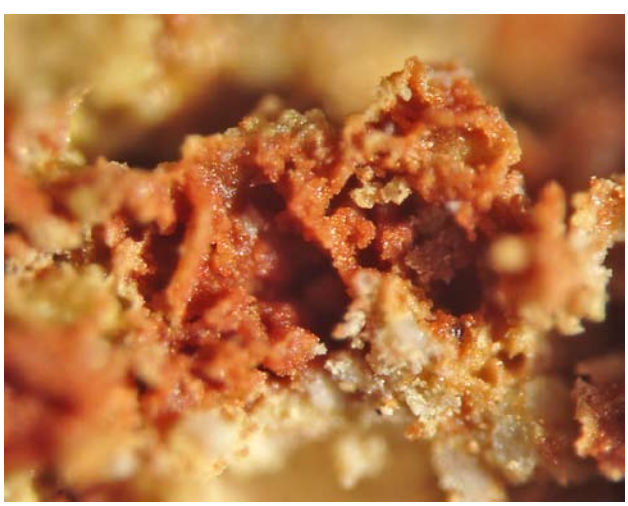

Fig. 21 Orange–red carminite aggregate with irregular surface. Krupka. Width of the area 1 mm. Photograph by J. Sejkora.

Tab. 7 Chemical composition of pharmacosiderite (wt. %)

	1	2	3	4	5	6
Na_2O	1.78	2.00	1.43	2.00	1.58	1.44
K_2O	7.55	8.26	9.64	9.86	10.03	10.13
CaO	0.22	0.15	0.13	0.10	0.14	0.25
BaO	0.19	0.26	0.18	0.07	0.23	0.23
ZnO	0.06	0.35	0.40	0.38	0.51	0.39
Al_2O_3	2.99	2.84	2.37	2.73	2.80	2.97
Fe_2O_3	32.07	34.75	34.91	34.22	32.75	31.04
SiO_2	1.21	1.78	1.15	1.54	1.15	1.74
As_2O_5	36.65	39.64	40.00	40.30	38.21	34.65
P_2O_5	0.11	0.08	0.05	0.02	0.23	0.15
F	0.09	0.09	0.08	0.09	0.09	0.08
H_2O*	18.30	19.73	19.65	19.84	19.13	18.25
Total	101.22	109.92	109.98	111.16	106.84	101.32
Na^+	0.506	0.516	0.377	0.515	0.431	0.419
K^+	1.412	1.401	1.669	1.668	1.800	1.939
Ca^{2+}	0.034	0.022	0.019	0.014	0.021	0.040
Ba^{2+}	0.011	0.013	0.009	0.004	0.013	0.013
Zn^{2+}	0.007	0.034	0.040	0.037	0.053	0.043
Σ K-site	1.970	1.986	2.114	2.239	2.317	2.455
Al^{3+}	0.516	0.444	0.380	0.427	0.465	0.526
Fe^{3+}	3.538	3.476	3.566	3.415	3.467	3.507
Σ Fe-site	4.054	3.920	3.945	3.841	3.932	4.033
Si^{4+}	0.177	0.236	0.156	0.204	0.162	0.261
As^{5+}	2.809	2.755	2.839	2.793	2.811	2.719
P^{5+}	0.014	0.008	0.005	0.002	0.027	0.020
Σ T-site	3.000	3.000	3.000	3.000	3.000	3.000
H^+	17.893	17.495	17.792	17.546	17.954	18.273
F^-	0.042	0.040	0.035	0.036	0.040	0.038
$(OH)^-$	4.896	4.495	4.790	4.549	4.956	5.269
Σ (OH)-site	4.938	4.534	4.824	4.585	4.996	5.307
H_2O	6.498	6.500	6.501	6.498	6.499	6.502

1–6 – representative spot analyses of pharmacosiderite from Krupka. Coefficients of empirical formula were calculated on the basis of (P + As + Si) = 3;
*H_2O content was calculated from the ideal content in the formula H_2O = 6.5 and charge balance.

Carminite was identified by X-ray powder diffraction. Its refined unit-cell parameters, a = 16.586(6), b = 7.583(4), c = 12.257(4) Å and V =1541.6(8) Å^3, are in agreement with the data published by Finney (1963), Kharisun et al. (1996) and Olmi and Sabelli (1995). The chemical composition of the studied mineral (Tab. 8) corresponds to carminite with somewhat elevated phosphorus contents in the tetrahedral sites corresponding to 0.11–0.16 *apfu* P (PAs_{-1} substitution). Empirical formula for carminite (average of three spot analyses) calculated on the basis (As + P + Si + S) = 2 is: $(Pb_{1.17}Ca_{0.02})_{\Sigma 1.19}(Fe_{1.83}Zn_{0.07}Al_{0.04}Cu_{0.02})_{\Sigma 1.96}[(AsO_4)_{1.82}(PO_4)_{0.14}(SiO_4)_{0.03}(SO_4)_{0.01}]_{\Sigma 2.00}[(OH)_{2.16}Cl_{0.01}]_{\Sigma 2.17}$.

Fig. 22 Surface of carminite aggregate composed of elongated tabular crystals. Krupka. Width of the area 30 µm. The BSE photograph by J. Sejkora.

Tab. 8 Chemical composition of carminite (wt. %)

	mean	1	2	3
CaO	0.19	0.16	0.17	0.24
PbO	38.01	38.77	40.07	35.20
CuO	0.21	0.00	0.36	0.26
ZnO	0.86	0.85	0.63	1.12
Al_2O_3	0.33	0.13	0.09	0.76
Fe_2O_3	21.20	21.11	21.12	21.37
SiO_2	0.30	0.00	0.00	0.89
As_2O_5	30.40	30.60	29.87	30.72
P_2O_5	1.35	1.34	1.58	1.13
SO_3	0.15	0.19	0.13	0.14
Cl	0.04	0.05	0.03	0.03
H_2O*	2.83	2.82	3.04	2.64
O=Cl	-0.01	-0.01	-0.01	-0.01
Total	95.86	96.01	97.08	94.49
Ca^{2+}	0.023	0.020	0.022	0.028
Pb^{2+}	1.173	1.208	1.265	1.052
Σ Pb-site	1.197	1.228	1.286	1.081
Cu^{2+}	0.018	0.000	0.032	0.022
Zn^{2+}	0.073	0.073	0.054	0.092
Al^{3+}	0.044	0.018	0.012	0.100
Fe^{3+}	1.829	1.839	1.863	1.786
Σ Fe-site	1.964	1.929	1.962	1.999
Si^{4+}	0.034	0.000	0.000	0.099
As^{5+}	1.822	1.852	1.831	1.784
P^{5+}	0.131	0.132	0.157	0.106
S^{6+}	0.013	0.017	0.012	0.011
Σ T-site	2.000	2.000	2.000	2.000
Cl^-	0.007	0.009	0.007	0.006
$(OH)^-$	2.164	2.177	2.378	1.956

Mean and 1–3 spot analyses of carminite from Krupka.
Coefficients of empirical formula were calculated on the basis of (P + As + Si + S) = 2;
*H_2O content was calculated from charge balance.

5.5. Cesàrolite

Cesàrolite is very rare as hemispherical microscopic aggregates 20–40 µm in diameter. It occurs in association with minerals of the beudantite–segnitite series and carminite. Owing to minimal size and quantity, this mineral could not be identified by X-ray diffraction. Chemical composition (Tab. 9) closely corresponds to the cesàrolite ideal formula $PbMn^{4+}{}_3O_6(OH)_2$ presented by Anthony et al. (1997). In the sample from Krupka, the Pb-site

Tab. 9 Chemical composition of cesàrolite (wt. %)

	mean	1	2	3	4
CaO	0.15	0.19	0.15	0.09	0.17
BaO	0.02	0.00	0.02	0.00	0.06
MgO	0.01	0.00	0.03	0.00	0.00
PbO	29.98	30.97	28.74	29.85	30.36
CuO	3.28	3.54	3.25	3.66	2.66
ZnO	0.18	0.20	0.18	0.16	0.20
Al_2O_3	0.99	1.44	0.85	0.59	1.09
Fe_2O_3	0.72	0.55	0.17	1.40	0.75
MnO_2	57.67	58.27	57.88	58.07	56.48
SiO_2	0.07	0.02	0.15	0.12	0.00
As_2O_5	2.36	3.13	1.67	1.91	2.72
P_2O_5	0.09	0.19	0.04	0.08	0.05
SO_3	0.06	0.02	0.03	0.15	0.04
Cl	0.07	0.05	0.08	0.05	0.08
O=Cl	–0.01	–0.01	–0.02	–0.01	–0.02
H_2O*	4.71	4.83	4.64	4.70	4.64
Total	100.34	103.39	97.86	100.81	99.28
Ca^{2+}	0.012	0.015	0.012	0.007	0.014
Ba^{2+}	0.001	0.000	0.001	0.000	0.002
Mg^{2+}	0.001	0.000	0.003	0.000	0.000
Pb^{2+}	0.598	0.599	0.585	0.592	0.616
Cu^{2+}	0.183	0.192	0.185	0.204	0.152
Zn^{2+}	0.010	0.010	0.010	0.009	0.011
Al^{3+}	0.087	0.122	0.076	0.051	0.097
Fe^{3+}	0.040	0.030	0.010	0.078	0.042
Σ Pb-site	0.932	0.969	0.882	0.940	0.934
Mn^{4+}	2.954	2.893	3.026	2.958	2.943
Si^{4+}	0.005	0.001	0.011	0.009	0.000
As^{5+}	0.091	0.117	0.066	0.074	0.107
P^{5+}	0.006	0.012	0.002	0.005	0.003
S^{6+}	0.003	0.001	0.002	0.008	0.002
Σ Mn-site	3.060	3.025	3.108	3.054	3.055
Cl^-	0.008	0.006	0.010	0.006	0.011
$(OH)^-$	2.326	2.314	2.344	2.313	2.332
Σ OH-site	2.334	2.320	2.354	2.319	2.343

Mean and 1– 4 – spot analyses of cesàrolite from Krupka.
Coefficients of empirical formula were calculated on the basis of all determined elements = 4;
*H_2O content was calculated from the charge balance.

contains in addition to dominant Pb (0.59–0.62 *apfu*) elevated contents of Cu (max. 0.20), Al (max. 0.12) and Fe (up to 0.08 *apfu*). The empirical formula of the studied cesàrolite (average of four spot analyses) calculated on the basis of a total of all determined metal and semi-metal elements = 4 is: $(Pb_{0.60}Cu_{0.18}Al_{0.09}Fe_{0.04}Ca_{0.01}Zn_{0.01})_{\Sigma 0.93}$ $(Mn_{2.95}As_{0.09}Si_{0.01}P_{0.01})_{\Sigma 3.06}O_6[(OH)_{2.33}Cl_{0.01}]_{\Sigma 2.34}$.

7. Conclusions

Supergene mineral association with abundant Cu-rich members of beudantite–segnitite series (alunite supergroup) occurs in the Krupka deposit, the Krušné hory Mountains, Czech Republic. The association includes mimetite, scorodite, pharmacosiderite, cesàrolite and carminite. Refined unit-cell parameters and quantitative chemical analyses for these minerals are reported. The following sequence of crystallization of supergene minerals was determined: mimetite → beudantite–segnitite → pharmacosiderite, scorodite, cesàrolite and carminite.

Copper-rich members of the beudantite–segnitite series from the Krupka ore deposit are notable for their as yet highest measured copper contents (up to 0.90 *apfu* Cu). Comparably high Cu contents were previously reported only for As-poor and S-rich members of alunite supergroup (plumbojarosite–beaverite series). The analytical data prove that Cu^{2+} enters the B^{3+} site according to a heterovalent substitution $Fe^{3+}Cu^{2+}_{-1} \rightarrow (AsO_4)^{3-}(SO_4)^{2-}_{-1}$. The X-ray powder patterns and refined unit-cell parameters are in good agreement with data published for minerals of the beudantite–segnitite series. The elevated Cu contents have no distinct influence on unit-cell parameters.

Acknowledgements The authors thank R. Škoda (Masaryk University, Brno) and J. Ederová (Institute of Chemical Technology, Prague) for their help in analytical works and S. Vrána (Czech Geological Survey, Prague) in preparation of the manuscript. The reviewers, Uwe Kolitsch and Stuart J. Mills, provided helpful comments on the manuscript which greatly improved its quality. This work was supported by Ministry of Culture of the Czech Republic, Project No. DE07P04OMG004.

Electronic supplementary material. The GPS coordinates of the studied samples are available online at the Journal web site *(http://dx.doi.org/10.3190/jgeosci.055)*.

References

Alpers CN, Nordstrom DK, Ball JW (1989) Solubility of jarosite solid solution precipitated from acid mine waters, Iron Mountain, California. Scie Geol Bull 42: 281–298

Anthony JW, bideaux RA, Bladh KW, Nichols MC (1997) Handbook of Mineralogy, Volume III, Halides, Hydroxides, Oxides. Mineral Data Publishing, Tucson, Arizona, pp 1–628

Baker WE (1966) An X-ray diffraction study of synthetic members of the pyromorphite series. Amer Miner 51: 1712–1721

Behrens EA, Sylvester P, Clearfield A (1998) Assessment of a sodium nonatitanate and pharmacosiderite-type ion exchangers for strontium and cesium removal from DOE waste simulants. Environ Sci Technol 32: 101–107

Birch WD, Pring A, Gatehouse BM (1992) Segnitite, $PbFe_3H(AsO_4)_2(OH)_6$, a new mineral in the lusungite group from Broken Hill, New South Wales, Australia. Amer Miner 77: 656–659

Bischoff W (1999) Segnitit von St. Andreasberg im Harz. Aufschluss 50: 102–104

Breidenstein B, Schlüter J, Gebhard G (1992) On beaverite: new occurrence, chemical data, and crystal structure. Neu Jb Mineral Mh 213–220

Buerger MJ, Dollase WA, Garaycochea-Wittke I (1967) The structure and composition of the mineral pharmacosiderite. Zeit Krist 125: 92–108

Burnham ChW (1962) Lattice constant refinement. Carnegie Inst Washington Year Book 61: 132–135

Dai Y, Hughes JM (1989): Crystal-structure refinements of vanadinite and pyromorphite. Canad Mineral 27: 189–192

Dai Y, Hughes JM, Moore PB (1991) The crystal structures of mimetite and clinomimetite, $Pb_5(AsO_4)_3Cl$. Canad Mineral 59: 369–376

De Bruiyn H, Van Der Westhuizen WA, Beukes GJ, Meyer TQ (1990) Corkite from Aggeneys, Bushmanland, South Africa. Mineral Mag 54: 603–608

Dutrizac JE, Dinardo O (1983) The co-precipitation of copper and zinc with lead jarosite. Hydrometallurgy 11: 61–78

Dutrizac JE, Jambor JL (2000) Jarosites and their application in hydrometallurgy. Rev Miner Geochem 40: 405–452

Dutrizac JE, Hardy DJ, Chen T (1996) The behaviour of cadmium during jarosite precipitation. Hydrometallurgy 41: 269–285

Dzikowski TJ, Groat LA, Jambor JL (2006) The symmetry and crystal structure of gorceixite, $BaAl_3[PO_3(O,OH]_2(OH)_6$, a member of the alunite supergroup. Canad Mineral 44: 951–958.

Farmer VC (1974) The Infrared Spectra of Minerals. Mineral Soc Monograph 4: 1–539

Finney JJ (1963) The crystal structure of carminite. Amer Miner 48: 1–13

Frost RL, Weier ML, Martens WN, (2005a) Thermal decomposition of jarosites of potassium, sodium and lead. J Thermal Anal Calorim 82: 115–118

Frost RL, Wills RA, Martens WN (2005b) Raman spectroscopy of beaverite and plumbojarosite. J Raman Spectrosc 36: 1106–1112

Frost RL, Wills RA, Weier ML, Musumeci AW, Martens WN (2005c) Thermal decomposition of natural and synthetic plumbojarosites: importance in "archeochemistry". Thermochim Acta 423: 30–35

Frost RL, Wills RA, Martens WN (2006) A Raman spectroscopic study of selected natural jarosites. Spectrochim Acta 63: 1–8

Frost RL, Locke AJ, Martens WN (2008) Thermal analysis of beaverite in comparison with plumbojarosite. J Thermal Anal Calorim 92: 887–892

Giusepetti G, Tadini C (1989) Beudantite $PbFe_3(SO_4)(AsO_4)(OH)_6$, its crystal structure, tetrahedral site disordering and scattered Pb distribution. Neu Jb Mineral, Mh 27–33

Grey IE, Mumme WG, Bordet P, Mills SJ (2008) A new crystal-chemical variation of the alunite-type structure in monoclinic $PbZn_{0.5}Fe_3(AsO_4)_2(OH)_6$. Canad Mineral 46: 1355–1364

Grey IE, Mumme WG, Mills SJ, Birch WD, Wilson NC (2009) The crystal chemical role of Zn in alunite-type minerals: structure refinements for kintoreite and zincian kintoreite. Amer Miner 94: 676–683

Hashimoto H, Matsumoto T (1998) Structure refinements of two natural pyromorphites $Pb_5(PO_4)_3Cl$, and crystal chemistry of chlorapatite group. Z Krist 146: 241–259

Jansa J, Novák F, Pauliš P, Scharmová M (1998) Supergene minerals of the Sn-W deposit Cínovec, Krušné hory mountains (Czech Republic). Bull mineral-petrolog Odd Nár Muz (Praha) 6: 83–112 (in Czech)

Jambor JL, Dutrizac JE (1983) Beaverite–plumbojarosite solid solutions. Canad Mineral 21: 101–113

Jambor JL, Dutrizac JE (1985) The synthesis of beaverite. Canad Mineral 23: 47–51

Jiang H, Lawson F (2006) Reaction mechanism for the formation of ammonium jarosite. Hydrometallurgy 82: 195–198

Keller P (1971): Kristallchemie der Phosphat- und Arsenat-Minerale unter besonder Berücksichtigung der Kationen-Koordinationspolyeder und des Kristallwassers. Teil. I: Die Anionen der Phosphat- und Arsenatminerale. Neu Jb Mineral, Mh 491–510

Kharisun, Taylor MR, Bevan DJM, Pring A (1996) The crystal structure of carminite: refinement and bond valence calculations. Mineral Mag 60: 805–811

Klingelhöfer G, Morris RV, Bernhardt B, Schröder C, Rodinov DS, De Souza PA, Yen A, Gellert R, Evlanov EN, Zubkov B, Foh J, Bonnes U, Kankeleit E, Gütlich P, Ming DW, Renz F, Wdowiak t, Squyres SW, Arvidson RE (2004) Jarosite and hematite at Meridiani Planum from Opportunity´s Mössbauer spectrometer. Science 306: 1740–1745

Kolitsch U, Pring A (2001) Crystal chemistry of the crandallite, beudantite and alunite groups: a review and evaluation of the suitability as storage materials for toxic metals. J Miner Petrol Sciences 96: 67–78

Libowitzky E (1999) Correlation of O–H stretching frequencies and O–H…O hydrogen bond lengths in minerals. Monatshefte Chem 130: 1047–1059

Mills SJ (2007) The crystal chemistry and geochronology of secondary minerals from the Broken Hill deposit, New South Wales. Unpublished Ph.D. thesis, University of Melbourne, Melbourne, Australia, pp 1–249

Mills SJ, Grey IE, Mumme WG, Miawaki R, Matsubara S, Bordet P, Birch WD, Raudsepp M (2008) Kolitschite, $Pb[Zn_{0.5}\square_{0.5}]Fe_3(AsO_4)_2(OH)_6$, a new mineral from the Kintore opencut, Broken Hill, New South Wales. Austral J Mineral 14: 63–67

Mills SJ, Hatert F, Nickel EH, Ferraris G (2009a) The standardisation of mineral group hierarchies: application to recent nomenclature proposals. Eur J Mineral 21: 1073–1080

Mills SJ, Kampf AR, Raudsepp M, Christy AG (2009b) The crystal structure of Ga-rich plumbogummite from Tsumeb, Namibia. Mineral Mag 73: 837–845

Mills SJ, Madsen IC, Grey IE, Birch WD (2009c) *In situ* XRD study of the thermal decomposition of natural arsenian plumbojarosite. Canad Mineral 47: 683–696

Morin G, Juillot F, Ildefonse P, Calas G, Samama JC, Chevallier P, Brown JG (2001) Mineralogy of lead in a soil developed on a Pb-mineralized sandstone (Largentière, France). Amer Miner 86: 92–104

Morris RC (1962) Osarizawaite from Western Australia. Amer Miner 47: 1079–1093

Murphy PJ, Smith AML, Hudson-Edwards KA, Dubbin WE, Wricht K (2009) Raman and IR spectroscopic studies of alunite-supergroup compounds containing Al, Cr^{3+}, Fe^{3+} and V^{3+} at the *B* site. Canad Mineral 47: 663–681

Mutter G, Eysel W, Greis O, Schmetzer K (1984) Crystal chemistry of natural and ion-exchanged pharmacosiderites. Neu Jb Mineral, Mh 4: 183–192

Myneni SCB, Traina SJ, Waychunas GA, Logan TJ (1998) Experimental and theoretical vibrational spectroscopic evaluation of arsenate coordination in aqueous solutions, solids, and at mineral–water interfaces. Geochim Cosmochim Acta 62: 3285–3300

Nambu M, Tanida K, Kano S (1964) Corkite from the Osarizawa mine, Akita Prefecture. Japan Assoc Mineral Petrol Econ Geol 52: 113–121

Novák F, Jansa J, Prachař I (1994) Classification and nomenclature of alunite–jarosite and related mineral groups. Věst Čes geol úst 69: 51–58

Olmi F, Sabelli C (1995) Carminite from three localities of Sardinia (Italy): crystal structure refinements. Neu Jb Mineral, Mh 553–562

Ondruš P (1993) ZDS – A computer program for analysis of X-ray powder diffraction patterns. Materials Science Forum, 133–136: 297–300, EPDIC-2. Enchede

Ondruš P, Skála R (1997) New quasi-empirical channel Search/Match algorithm for ICDD PDF2 Database: a tool for qualitative phase analysis integrated in the ZDS-System software package for X-ray powder diffraction analysis. In: Fifth European Powder Diffraction Conference EPDIC-5. Parma, pp 193

Ózacar M, Alp A, Aydin AO (2000) Kinetics of thermal decomposition of plumbojarosite. J Thermal Anal Calorim 59: 869–875

Pe-Piper G, Dolansky LM (2005) Early diagenetic origin of Al phosphate–sulphate minerals (woodhouseite and crandallite series) in terrestrial sandstones, Nova Scotia, Canada. Amer Miner 90: 1434–1441

Peacor DR, Dunn PJ (1985) Sodium-pharmacosiderite, a new analog of pharmacosiderite from Australia and new occurrences of barium-pharmacosiderite. Miner Record 16: 121–124

Plášil J, Sejkora J, Čejka J, Škácha P, Goliáš V (2009a) Supergene mineralization of the Medvědín uranium deposit, Krkonoše Mountains, Czech Republic. J Geosci 54: 15–56

Plášil J, Čejka J, Sejkora J, Hloušek J, Goliáš V (2009b) New data for metakirchheimerite from Jáchymov (St. Joachimsthal), Czech Republic. J Geosci 55: 373–384

Plášil J, Sejkora J, Čejka J, Škácha P (2009c) The question of water content at parsonsite: model case – occurrence at the Červené žíly vein system, the Jáchymov ore district, Czech Republic. J Geosci 55: 385–394

Pouchou JL, Pichoir F (1985) „PAP“ (φρZ) procedure for improved quantitative microanalysis. In: Armstrong JT (ed) Microbeam Analysis, San Francisco Press, pp 104–106

Pring A, Birch WD, Dawe J, Taylor M, Deliens M, Walenta K (1995) Kintoreite, $PbFe_3(PO_4)_2(OH,H_2O)_6$, a new mineral of the jarosite-alunite family, and lusungite discredited. Mineral Mag 59: 143–148

Rattray KJ, Taylor MR, Bevan DJM, Pring A (1996) Compositional segregation and solid solution in the lead-dominant alunite-type minerals from Broken Hill, N.S.W. Mineral Mag 60: 779–785

Sasaki K, Tanaike O, Konno H (1998) Distinction of jarosite-group compounds by Raman spectroscopy. Canad Mineral 36: 1225–1235

Sasaki K, Konno H (2000) Mineralogy of jarosite-group compounds precipitated from biologically and chemically oxidized Fe ions. Canad Mineral 38: 45–56

Sato E, Nazai I, Terada Y, Tsutsumi Y, Yokoyama K, Miawaki R, Matsubara S (2008) Study of Zn-bearing beaverite $Pb(Fe_2Zn)(SO_4)_2(OH)_6$ obtained from Mikawa mine, Niigata Prefecture, Japan. Jour Mineral Petrol Sci 103: 141–144

Schmetzer K, Horn W, Bank H (1981) Alumopharmakosiderit, $KAl_4[(OH)_4(AsO_4)_3]$ .6,5H_2O, ein neues Mineral. Neu Jb Mineral, Mh 3: 97–102

Schwab RG, Pimpl T, Schukow H, Stolle A, Breitinger DK (2004) Compounds of the crandallite-type: synthesis, properties and thermodynamic data of pure crandallite and woodhouseite. Neu Jb Mineral, Mh 385–409

Scott KM (1987) Solid solution in, and classification of, gossan-derived members of the alunite–jarosite family, northwest Queensland, Australia. Amer Miner 72: 178–187

Sejkora J, Breiter K (1999) The historical ore district Krupka, Krušné hory Mountains. Bull mineral-petrolog Odd Nár Muz (Praha) 7: 29–45 (in Czech)

Sejkora J, Škovíra J (2007) The occurrence of cyantrichite at mine dumps of the Krupka ore deposit, Krušné hory Mountains. Bull mineral-petrolog Odd Nár Muz (Praha) 14-15: 126–127 (in Czech)

Sejkora J, Čejka J, Šrein V (2001a) Pb dominant members of crandallite group from Cínovec and Moldava deposits, Krušné hory Mts. (Czech Republic). J Czech Geol Soc 46: 53–67

Sejkora J, Houzar S, Šrein V (2001b) Segnitite from Štěpánov nad Svratkou, western Moravia. Acta Mus Moraviae, Sci geol 86: 85–92 (in Czech)

Sejkora J, Čejka J, Šrein V (2007a) Supergene uranium mineralization from Horní Halže near Měděnec (Krušné hory Mountains), Czech Republic. J Geosci 52: 199–210

Sejkora J, Hawthorne FC, Cooper MA, Grice JD, Vajdak J, Jambor JL (2009) Burgessite, $Co_2(H_2O)_4[AsO_3(OH)]_2(H_2O)$, a new arsenate mineral species from the Kelly mine, South Lorrain township, Ontario, Canada. Canad Mineral 47: 159–164

Sejkora J, Ondruš P, Fikar M, Veselovský F, Mach Z, Gabašová A, Škoda R, Beran P (2006a) Supergene minerals at the Huber stock and Schnöd stock deposits, Krásno ore district, the Slavkovský les area, Czech Republic. J Czech Geol Soc 51: 57–101

Sejkora J, Škoda R, Ondruš P, Beran P, Süsser C (2006b) Mineralogy of phosphate accumulations in the Huber stock, Krásno ore district, Slavkovský les area, Czech Republic. J Geosci 51: 103–147

Sejkora J, Škovíra J, Škoda R (2007b) Mineral of the mixite group from deposit Krupka, Krušné hory Mountains. Bull mineral-petrolog Odd Nár Muz (Praha) 14–15: 128–130 (in Czech)

Sejkora J, Škovíra J, Škoda R (2008) Zincolivenite from the ore district Krupka, the Krušné hory Mts., Czech Republic. Bull mineral-petrolog Odd Nár Muz (Praha) 16: 24–29 (in Czech)

Slansky E (1977) Plumbogummite from Ivanhoe Mine, Northern Territory, Australia. Neu Jb Mineral, Mh 45–53

Szymański JT (1988) The crystal structure of beudantite, $Pb(Fe,Al)_3[(As,S)O_4]_2(OH)_6$. Canad Mineral 26: 923–932

Škovíra J, Sejkora J, Dvořák Z, Řehoř M (2004) New informations about supergene minerals from the Krupka ore district (Krušné hory Mountains). Bull mineral-petrolog Odd Nár Muz (Praha) 12: 228–232 (in Czech)

Števko M, Ozdín D, Bačík P, Pršek J, Gramblička R (2008) Secondary minerals from the base metals mineralization near Valaská Belá, Slovak Republic. Bull mineral-petrolog Odd Nár Muz (Praha) 16: 177–184 (in Slovak)

Taguchi Y (1961) On osarizawaite, a new mineral of the alunite group from the Osarizawa mine, Japan. Mineral J Japan 3: 181–194

Taguchi Y, Kizawa Y, Okada N (1972) On beaverite from Osarizawa mine. Kobutsugaki Zasshi (Japan) 10: 313–325

Vansant FK, Van Der Veken BJ, Desseyn HO (1973) Vibrational analysis of arsenic acid and its anions. I. Description of the Raman spectra. J Mol Struct 1: 425–437

Van Tassel R (1958) Jarosite, natrojarosite, beaverite, leonhardtite, et hexahydrite du Congo belge. Inst Roy Sci Nat Belge Bull 34: 1–12

Walenta K (1966) Beiträge zur Kenntniss seltener Arsenatmineralien unter besonderer Berücksichtigung von Vorkommen des Schwarzwaldes. Tschermaks Mineral Petr Mitt 11: 121–161

Walenta K, Zwiener M, Dunn PJ (1982) Philipsbornit, ein neues Mineral der Crandallitreihe von Dundas auf Tasmanien. Neu Jb Mineral, Mh 1–5

Yakovenchuk VN, Selivanova EA, Ivanyuk GY, Pakhomovsky YA, Spiridonova DV, Krivovichev SV (2008) First natural pharmacosiderite-related titanosilicates and their ion-exchange properties. In: Krivovichev S (ed) Minerals and Advanced Materials I. Springer, Berlin, pp 27–35